A Multi-Output Machine Learning Approach to Sorption-Enhanced Steam Methane Reforming

Ekene E. Iwuchukwu and Adegboyega B. Ehinmowo*
Petroleum and Gas Engineering, University of Lagos, Lagos, Nigeria

Abstract

Sorption-enhanced steam methane reforming (SE-SMR) provides the added advantage of CO_2 capture compared to conventional steam methane reforming, limited by CO_2 emissions. Current SE-SMR machine learning models primarily focus on predicting methane conversion and hydrogen production, but overlook carbon dioxide capture and hydrogen purity. This limitation reduces their effectiveness for real-time applications, where it is crucial to balance trade-offs involving environmental, economic, and technical objectives. This research employs a dual multi-output framework to predict methane conversion, hydrogen yield, hydrogen purity, and carbon dioxide capture using Linear Regression, Support Vector Machine, Decision Tree, Random Forest, CatBoost, and LightGBM models. Most models demonstrated high prediction accuracy, characterised by high R^2 and low root mean square error (RMSE) values. Support Vector Machine (SVM) performed the best in predicting methane conversion, hydrogen yield, and hydrogen purity, achieving R^2 values of 0.993, 0.988, and 0.979, respectively. Random forest performed well in all models, but achieved its best results in predicting carbon dioxide capture, with an R^2 value of 0.996 and an RMSE of 2.059%. This study presents a reliable technique for predicting hydrogen production from SE-SMR integrated with carbon dioxide capture.

Keywords: *Hydrogen production, Carbon capture, Machine learning, Methane conversion, Energy.*

1. Introduction

Petroleum-based fuels such as coal, crude oil, and natural gas are the largest energy sources, constituting 81% of the global energy mix in 2023 [1]. However, fossil fuels are not clean energy sources. The combustion of coal, crude oil, and natural gas releases carbon dioxide, which is a greenhouse gas known to contribute to climate change. The devastating effects of climate change include global warming, heavy precipitation, and increased droughts [2-3]. Fossil fuels contribute the largest percentage to climate change, with almost 90% of global CO_2 emissions and 75% of greenhouse gases produced worldwide [4]. Consequently, there is a global clamour for transitioning from petroleum-based fuels to renewable energy.

The adoption of renewable energy has increased in recent years. An increase in solar and wind power use from 0.2% in 2000 to 13.4% in 2023 drove electricity generation from renewable energy to 30% in 2023 [5]. However, many renewable energy resources are still in their developmental stages and have limitations. Hydrogen energy effectively solves some of these limitations, making it a suitable candidate for meeting the future world energy demand.

Hydrogen has a high energy density and is independent of weather [6], solving the low energy

* Corresponding author. Tel.: +2348033698638
E-mail address: aehinmowo@unilag.edu.ng

Manuscript History:
Received 19 October, 2025, Revised 24 May, 2026, Accepted 25 May, 2026, Published 31 October, 2026
Copyright © 2026 UNIMAS Publisher. This is an open access article under the CC BY-NC-SA 4.0 license.
https://doi.org/10.33736/jaspe.11153.2026

e-ISSN: 2289-7771

density and power intermittency problem in solar and wind energy. Adopting hydrogen energy eliminates the requirement for the presence of a river and the elevation associated with hydro-energy. The advantage of hydrogen in addressing crucial limitations of other renewable energy sources necessitates the optimisation of hydrogen production.

Several methods produce hydrogen, including electrolysis, biomass gasification, steam reforming, and partial oxidation. However, steam methane reforming is the primary method to produce hydrogen, accounting for 50% of global hydrogen production [7]. A major limitation of steam methane reforming (SMR) is the emission of over seven times as much CO_2 as the H_2 produced [8]. Therefore, the process needs optimisation to reduce its effect on the environment.

Sorption-enhanced steam methane reforming (SE-SMR) uses a solid sorbent to capture CO_2. Consequently, CO_2 emissions are reduced, and the equilibrium position is shifted to enhance the methane conversion efficiency and hydrogen purity [9-10]. An additional advantage of SE-SMR over conventional SMR is the operating temperature reduction to 500℃ – 700℃ compared to the high temperature of 700℃ – 1000℃ required in traditional steam methane reforming. Thereby, reducing the energy requirement of the process [11–13].

Machine learning algorithms can predict process outputs, optimise operational parameters, and provide real-time adjustments in hydrogen production. As a result, many research works have implemented machine-learning models in different hydrogen processes, including fermentation, gasification, and reformation.

Hosseinzadeh et al. [14] applied four machine learning models: AdaBoost, Random Forest (RF), Support Vector Machine (SVM), and gradient boosting machine (GBM) to evaluate hydrogen production from wastewater using dark fermentation. The coefficient of determination or R^2 for each model was 0.889, 0.902, 0.885, and 0.893, respectively. Although the random forest model produced the highest prediction accuracy, all models indicated operational precision.

Ozbas et al. [15] used time, temperature, CO, CO_2, CH_4, O_2, and heating value as model parameters to predict hydrogen concentration in biomass gasification using Linear Regression, K-Nearest Neighbours, Support Vector Machine, and Decision Tree models. The models produced high R^2 values of 0.999, 0.991, 0.997, and 0.991, respectively. Advanced optimisation algorithms such as Levenberg-Marquardt, Bayesian optimisation, and the Firefly algorithm can be integrated with supervised and unsupervised machine learning models for effective hyperparameter tuning and fast convergence.

Alsaffar et al. [16] integrated Bayesian regularisation and Levenberg-Marquardt with an artificial neural network to predict hydrogen production in thermo-catalytic methane decomposition. The Levenberg-Marquardt-trained neural network performed better than the neural network integrated with Bayesian regularisation.

Machine learning has also been successfully applied in sorption-enhanced steam methane reforming. Nkulikiyinka et al. [17] utilised input process characteristics, including temperature, pressure, steam-to-carbon ratio, and sorbent-to-carbon ratio, to develop random forest and artificial neural network models for predicting hydrogen yield, methane conversion efficiency, and regenerator outputs. Both models predicted reformer hydrogen with similar accuracy, with an R^2 of 0.98. However, the random forest model performed better in predicting methane conversion.

Wang et al. [18] deployed various machine learning ensemble methods, including XGBoost, AdaBoost, and bagging, for hydrogen production prediction. Several input process variables, including temperature, pressure, gas velocity, and the ratio of steam to carbon, were considered. Among the models tested, XGBoost demonstrated superior performance, achieving a test R^2 value of 0.98264 for hydrogen yield prediction. Additionally, the XGBoost model effectively predicted methane conversion, attaining a test R^2 value of 0.96276. Similarly, Ehinmowo et al. [19] deployed various nonlinear machine learning models incorporating Levenberg-Marquardt, Bayesian optimisation, Firefly, and Differential Evolution algorithms to predict hydrogen yield and methane conversion. The research evaluated multiple models, with the support vector machine showing the greatest predictive accuracy for methane conversion, reaching an R^2 value of 96.5%. For hydrogen yield prediction, the CatBoost model outperformed others, achieving an R^2 value of 96.3%. However, hydrogen purity and carbon dioxide capture were not investigated.

More recently, Bishnu et al. (2025) [20] integrated a simulated annealing optimisation architecture with a random forest model to optimise SE-SMR for real-time applications. The result showed an

optimal methane conversion rate of 0.99979. While machine learning has been applied in the study of SE-SMR, most research primarily focuses on methane conversion and hydrogen yield, overlooking hydrogen purity and carbon dioxide capture. However, hydrogen purity and carbon dioxide capture are closely related and share similar thermodynamics [21]. Furthermore, many studies tend to isolate performance indicators, which prevents them from leveraging the interconnections between these indicators. This study adopts a dual multi-output framework to simultaneously predict methane conversion, hydrogen yield, hydrogen purity, and carbon dioxide capture. Thereby, addressing the gaps in the existing literature, improving prediction accuracy, and enhancing generalisation.

2. Methodology

2.1. Data collation and descriptive analysis

The data employed for this research were obtained from Antzara et al. [21] and Faheem et al. [22], who evaluated the effects of crucial process parameters on SE-SMR using Aspen Plus simulation software. Since the data were selected from different sources, some transformations were performed to ensure consistency. Firstly, the hydrogen yield values presented with respect to the theoretical hydrogen were converted to hydrogen yield values based on methane consumed. This transformation was performed because hydrogen yield based on feedstock consumed is a better indicator of process economics, as well as, to ensure consistency with the study of Faheem et al. Also, the pressure values presented in atm in the work of Antzara et al. were converted to bar to also maintain consistency with the work of Faheem et al. After all transformations, a total of 121 data points were employed for this study.

Table 1 shows the descriptive statistics of the data employed to predict the four process performance indicators. The dataset contained 121 data points. Reforming temperature, which is essential in SE-SMR, varied from 499.40℃ to 1199.72℃, averaging 691.61℃ and deviating from the mean by 121℃. This reflects a wide thermal distribution consisting of low and high temperatures. Reforming pressure ranged from 1.01– 40.01 bar, showing that the dataset considers traditional and high-pressure SE-SMR conditions.

Table 1. Statistical information about the data [21-22]

Parameters	Count	Mean	Standard deviation	Minimum	25%	50%	75%	Maximum
Reformer Temperature (℃)	121	691.6	121.18	499.4	650	650	700.03	1199.72
Reformer Pressure (bar)	121	8.54	11.38	1.01	1.01	1.01	15.22	40.01
S/C	121	3	0.51	1.01	3	3	3	4.98
CaO/C	121	0.95	0.17	0	1	1	1	1
Methane Conversion (%)	121	85.45	13.95	34.44	74.8	91.16	97.52	99.99
Hydrogen Yield (%)	121	84.4	13.51	20.61	77.01	89.49	93.49	97.56
Hydrogen Purity (%)	121	40.75	6.11	17.46	36.65	41.76	45.65	48.62
Carbon dioxide Capture (%)	121	52.52	32.5	0.01	24.43	68.47	77.17	90.57

The calcium oxide-to-carbon (CaO/C) ratio, a crucial factor in determining in situ CO_2 capture, had a mean of 0.95 and a maximum value of 1.00, indicating a focus on conditions rich in the sorbent. Steam-to-carbon (S/C) ratios were narrower, with a spread of 1.01 to 4.98 and a constant median of 3.00. The metrics on the process performance also indicated significant variation. The conversion of methane was 34.44 to 99.99%, and the mean conversion was 85.45% with a standard deviation of 13.95%. The large median of 91.16% indicates that most of the SE-SMR runs surpassed 90 conversion, which is in line with thermodynamic expectations under CO_2 removal. There was an

identical pattern in the case of hydrogen purity, values ranging between 20.61% and 97.56% with an 84.40% mean. The lower limit is a condition in which the sorbent saturation or methane slippage impacts the product gas quality.

Hydrogen yield ranged between 17.46% to 48.62%. It was observed that the distribution of carbon dioxide capture was the largest, with a standard deviation of 32.50%, a minimum of 0.01%, and a maximum of 90.57 %. The spread reflects heterogeneity in sorbent performance, which can be associated with the variation of the CaO/C ratio or kinetics. Overall, the data shows sufficient variability for implementing machine learning.

2.2. Data processing

The data consist of four input features: reformer temperature, reformer pressure, steam-to- carbon ratio, and sorbent-to-carbon ratio. Important variables such as residence time, catalyst properties were excluded due to unavailability in adopted dataset. Target variables were methane conversion, hydrogen yield, hydrogen purity, and carbon dioxide capture. The data was cleaned and preprocessed to ensure consistency in units and evaluation parameters. Also, outliers were removed to improve predictive accuracy.

Since the input features have different magnitudes, they were normalised to remove the effect of difference in magnitude using min-max scaling. Furthermore, to prevent the models from memorising any unnecessary patterns, the data was shuffled. Finally, the data was split for training and testing purposes using an 8:2 ratio to ensure that there is an unseen data to evaluate the generalisability of these models. Due to the small size and lack of variability of S/C and CaO in the dataset and to ensure that the models are trained in a manner that preserves the variation in the dataset, model robustness was evaluated by using the best hyperparameters that perform consistently and minimised the difference in performance metrics between train and test results.

2.3. Model framework

Methane conversion and hydrogen yield are driven by catalytic kinetics and thermodynamic equilibrium, while hydrogen purity and carbon dioxide capture are affected by adsorption-desorption dynamics [21, 22]. This bi-mechanistic nature is reflected in the correlation between the pairs. Consequently, a dual multi-output approach was implemented with the aim of leveraging the relationship between these pairs. Methane conversion and hydrogen yield were trained together, while hydrogen purity and carbon dioxide were modelled together. Bayesian Optimisation was used for tuning the hyperparameters.

2.4. Evaluation parameters

The following equations were used to express the target variables.

$$\mathrm{CH_4\,conversion}\ (\%) = \frac{nCH_{4_{in}} - nCH_{4_{out}}}{nCH_{4_{in}}} * 100 \quad (1)$$

Where $nCH_{4_{in}}$ is the number of moles at the inlet, and $nCH_{4_{out}}$ is the outlet methane molar amount.

$$H_2\ yield\ (\%) = \frac{mol.weight\ of H_2 * nH_{2_{out}}}{mol.weight\ of CH_4 * nCH_{4_{in}}} * 100 \quad (2)$$

Where $nH_{2_{out}}$ is the molar amount of H_2 produced

$$H_2\ purity\ (\%) = \frac{nH_{2_{out}}}{nCH_{4_{in}} + nH_{2_{out}} + nCO_{out} + nCO_{2_{out}}} * 100 \quad (3)$$

Where nCO_{out} *and* $nCO_{2_{out}}$ are the molar amounts of carbon monoxide and carbon dioxide produced respectively.

$$CO_2\ capture\ (\%) = \frac{nCH_{4_{in}} - nCH_{4_{out}} - nCO_{out} - nCO_{2_{out}}}{nCH_{4_{in}}} * 100 \quad (4)$$

2.5. Machine learning models used

2.5.1. *Linear Regression:* Linear regression employs a straight-line equation to represent observed data. This model was selected to serve as a baseline model to compare with more complex machine learning algorithms. Figure 1 shows the flowchart of a linear regression algorithm.

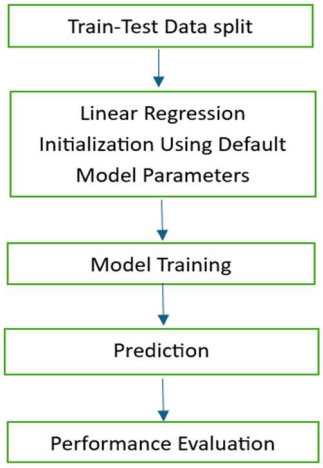


Figure 1. Flowchart showing the implementation of linear regression. Adapted from Costa et al. [23]

2.5.2. *Decision Tree:* Classification and regression problems often utilise the decision tree model. This approach systematically splits data into smaller subsets based on various attributes until a predetermined stopping condition is met [24]. This process results in a tree-like structure comprising a root node, decision nodes, and leaf nodes, as illustrated in Figure 2.

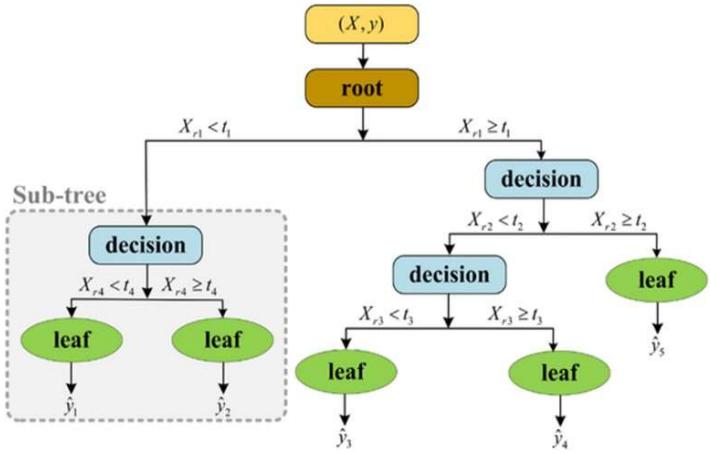


Figure 2. Diagram showing the tree-like splitting methodology of the decision tree model [25].

2.5.3. *Support Vector Machine:* Support Vector Machine is a supervised machine learning algorithm used for classification and regression problems. Its working principle aims to separate the data points in a feature space to find an optimal hyperplane, as shown in Figure 3.

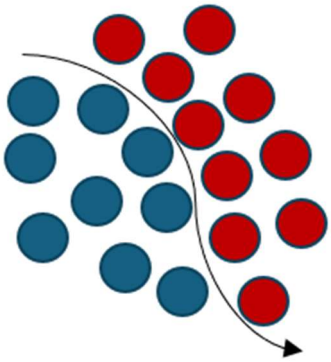


Figure 3. Diagram showing the hyperplane for splitting data points in SVM. Adapted from Manjrekar et al. [26]

2.5.4. *Random Forest:* This is an ensemble machine learning algorithm applicable to classification and regression problems and uses a combination of many decision trees to improve predictive accuracy. For regression tasks, the predictions from different trees are averaged to find the final prediction, as depicted in Figure 4.

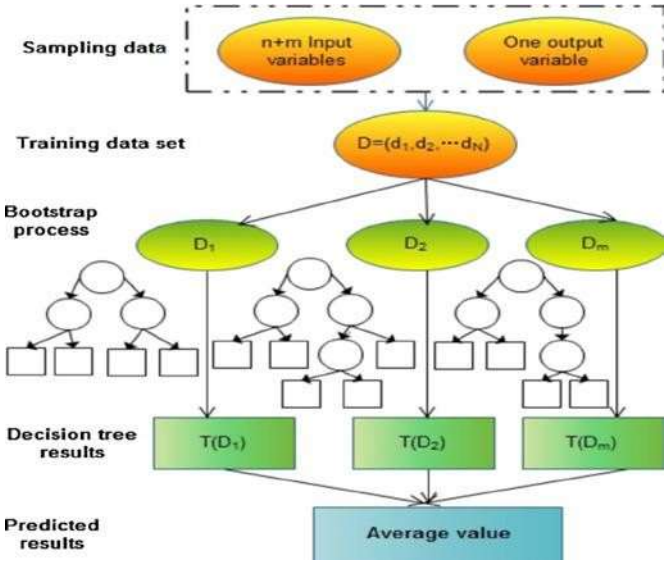


Figure 4. Flowchart showing random forest regression methodology [27].

2.5.5. *Categorical Boosting:* Gradient boosting is a method that constructs decision trees in sequence to minimise errors. Each subsequent tree enhances predictions by addressing the mistakes

of previous trees. CatBoost, a particular implementation of this technique, stands out from other boosting approaches due to its capacity to efficiently process categorical variables without the need for encoding. The algorithm's workflow is illustrated in Figure 5.

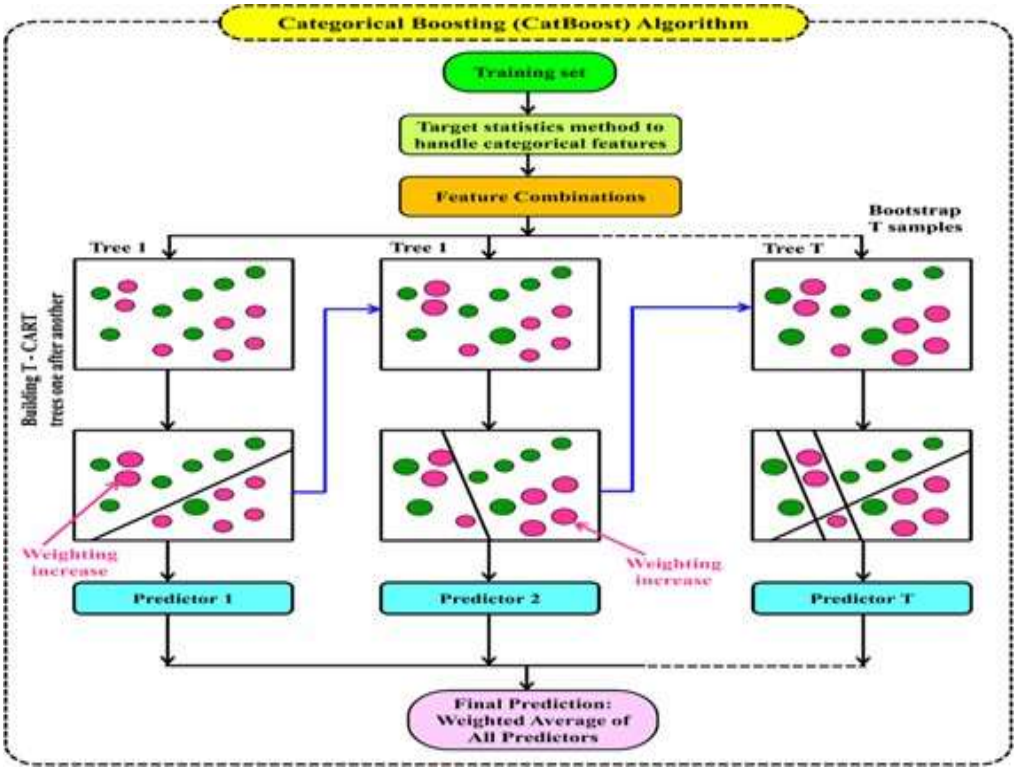


Figure 5. Flowchart depicting the implementation of the CatBoost algorithm [28]

2.5.6. *Light Gradient Boosting Machine:* LightGBM is used for both regression and classification problems. Rather than growing the trees based on level as in XGBoost, LightGBM grows the trees using the leaf. Figure 6 presents the LightGBM framework.

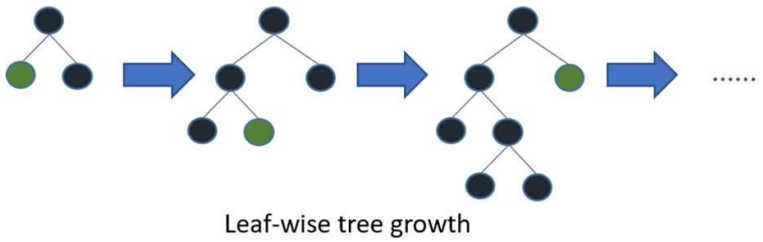


Figure 6**.** Flowchart showing the leaf-wise growth in LightGBM [29]

2.5.7. *Bayesian Optimisation:* Hyperparameter optimisation or tuning is essential in building accurate tree-based and boosting models. Bayesian optimisation is based on Bayes' theorem. It utilises a probability model to optimise hyperparameters, as well as an acquisition function to determine the next sample location, as shown in Figure 7. Consequently, this reduces the time

required for hyperparameter tuning and improves the performance of machine learning models.

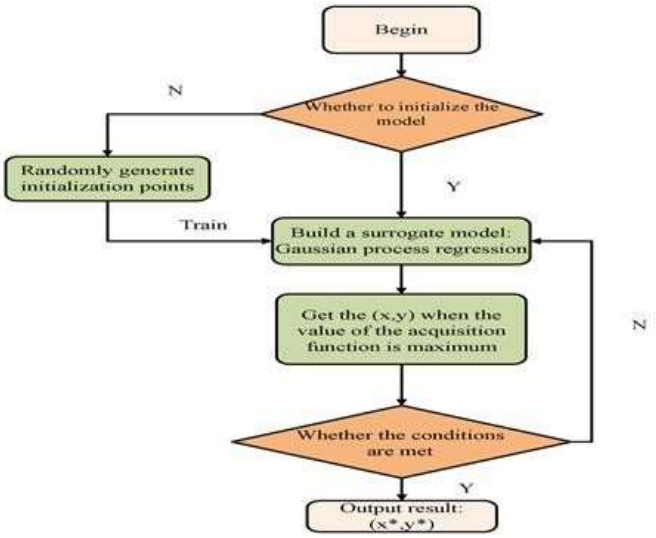


Figure 7. Flowchart depicting Bayesian Optimisation [30]

2.6. Model Performance Evaluation Metrics

Four evaluation metrics were used to assess the performance of the models:

2.6.1. Coefficient of Determination (R^2): This evaluation metric is also known as R-squared. It explains how well the model fits the data using the total variance. The higher its value, the more accurate the model.

$$R^2 = 1 - \frac{\sum_{i=1}^{n}(y_i - \hat{y})^2}{\sum_{i=1}^{n}(y_i - \bar{y})^2} \quad (5)$$

Where,
i = index of each data point
y_i = actual value in the data
$\hat{y}$ = predicted value in the data
n = total number of data points
$\bar{y}$ = average value in a sample

2.6.2. Root Mean Square Error (RMSE): It evaluates the level of accuracy of the model as a measure of the magnitude of deviation of the errors. Since it squares the errors, it is highly applicable in situations where large errors are unnecessary. RMSE produces a similar unit to the predicted variable. Thereby, ensuring easier interpretation.

$$RMSE = \sqrt{\frac{\sum_{i=1}^{n}(y_i - \hat{y})^2}{n}} \quad (6)$$

2.6.3. Mean Squared Error (MSE): This computes the average of the squared difference between the actual and predicted data. Similar to RMSE, it squares the error and is useful where large errors

are not required. The result of MSE is difficult to interpret since the error is the square of the predicted variable.

$$MSE = \frac{\sum_{i=1}^{n}(y_i - \hat{y})^2}{n} \quad (7)$$

2.6.4. Mean Absolute Error (MAE): This metric uses the absolute difference between the predictions and the actual values to evaluate the performance of the model. It is unfit for models where large errors are unsuitable, since it penalises all errors equally. The absolute nature of MAE eliminates directional error, which may be important in some situations.

$$MAE = \frac{\sum_{i=1}^{n}|y_i - \hat{y}|}{n} \quad (8)$$

2.6.5. Mean Absolute Percentage Error (MAPE): This describes the error as a percentage of the actual data. It is easy to understand and interpret. However, a problem arises when the actual data is zero. Similar to MAE, MAPE eliminates directional error.

$$MAPE = \sum_{i=1}^{n}\left|\frac{y_i - \hat{y}}{y_i}\right| * \frac{100}{n} \quad (9)$$

3. Results and Discussion

3.1. Correlation analysis

The Pearson correlation heat map that demonstrates the linear correlations of the important process variables and performance indicators on the SE-SMR system was presented in Figure 8.

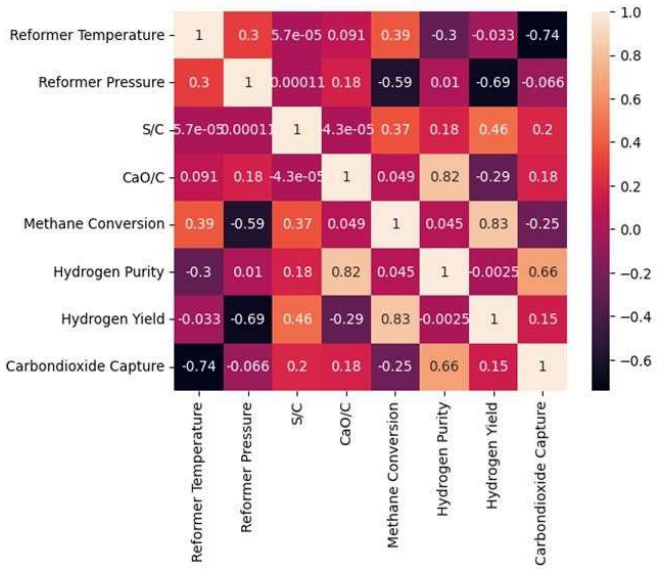


Figure 8. Correlation between process variables and performance Indicators.

The analysis offers profound considerations of the relationships that exist between the operating conditions: reformer temperature, reformer pressure, steam-to-carbon ratio, CaO/C ratio, and system outputs: methane conversion, hydrogen purity, hydrogen yield, and CO_2 capture.

Remarkably, reformer temperature and carbon dioxide capture efficiency show a strong negative correlation (r = -0.74). This negative correlation is indicative of the reduction in the carbonation reaction between CO_2 and CaO, as is known in the thermodynamic restrictions of CaO- based sorbents at higher temperatures [21, 22]. Therefore, conditions of operation within and beyond the optimum carbonation conditions can effectively limit the advantage of in-situ CO_2 extraction and thus cut short one of the fundamental benefits of SE-SMR.

On the other hand, a moderate positive correlation was provided between reformer temperature and methane conversion (r = 0.39), and a strong positive correlation between hydrogen yield and methane conversion (r = 0.83).

The CaO to C ratio (CaO/C) has a positive correlation with Hydrogen purity (r = 0.82) and CO_2 capture (r = 0.18), and thus represents the importance of excess sorbent to shift the equilibrium and enhance performance in terms of separation. The high correlation between CaO/C and H_2 purity together indicates that large amounts of CO_2 are removed during the reaction can creating an enriched product hydrogen stream, which is a typical characteristic of the SE-SMR process.

The pressure exerted by the reformers was found to negatively correlate with both methane conversion (r = -0.59) and hydrogen yield (r = -0.69) in compliance with Le Chatelier's principle, since higher pressures are more likely to favour the reactants in steam reforming. Conversely, its low correlation to hydrogen purity (r = 0.01) indicates a low determination of separation efficiency at the tested conditions.

Additionally, the S/C ratio was found to positively correlate with the methane conversion (r = 0.37) and hydrogen yield (r = 0.46), as also indicated in the literature, that a greater amount of steam was linked to better reforming kinetics and the rate of carbon deposition decreased [31]. Nevertheless, its modest effect on CO_2 capture (r = 0.18) reflects the secondary impact of steam dilution on partial pressures and sorption dynamics.

3.2. Distribution analysis

Figure 9 shows the distribution plot of all the operating variables and outputs in the SE-SMR dataset. The histograms, together with the aid of kernel density estimation (KDE), reflect skewness.

Reformer Temperature and Pressure

The reformer temperature distribution shows a moderately right-skewed profile, with most values concentrated between 600 and 700°C. This clustering reflects the typical operating range for optimal steam reforming reactions, balancing thermodynamic favorability with sorbent stability. However, the tail extending toward 1200°C indicates high-temperature conditions required for exploring thermal limits or simulating regeneration conditions.

Reformer pressure displays a highly skewed distribution, with the majority of data points below 10 bar, and a few outliers extending beyond 30 bar. This reflects an emphasis on low-pressure operation, which aligns with the need to favour product formation in endothermic reactions.

Steam-to-Carbon (S/C) and CaO/C Ratios

The S/C ratio distribution is also normal with a high peak and symmetrical at 3.0, which shows a controlled range of the steam in the data. Such a gregarious distribution is in line with the applied reforming practices that utilise less steam in an attempt to minimise the thermal duty, along with sustaining the life of a catalyst and ensuring hydrogen selectivity. Likewise, the CaO/C ratio has a strong peak at 1.0, which indicates a sorbent-rich condition, which is commonly employed to exploit in-situ CO_2 capture and increase H_2 purity.

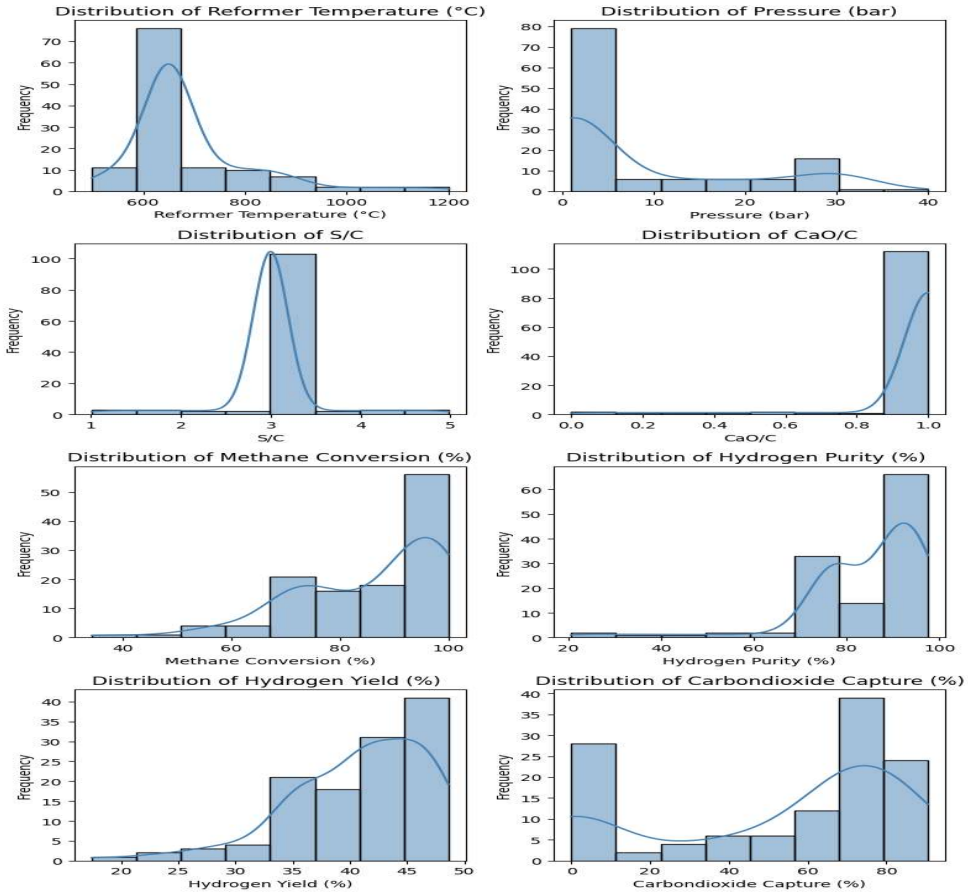


Figure 9. Distribution of process variables and performance indicators.

Process Performance Indicators

The conversion of methane has a skewed right distribution where the most common frequency is close to complete conversion. This implies that a majority of the operating conditions reached high levels of methane reforming due to the combined influence of elevated temperature and sufficient levels of steam supply. The same tendency is traced in hydrogen purity, which also reaches high levels, corresponding to the efficiency of removing CO_2 through the sorbent and balance-causing mechanisms present within SE-SMR.

The distribution of hydrogen yield is more spread, though there is a moderate skew around 45% toward the high side, which indicates that hydrogen production was overall effective. Lastly, the extent of carbon dioxide capture demonstrates a consistent dispersion, with significant density at low and high capture percentages.

3.3 Model evaluation study

The table 2-5 show the hyperparameter search space and best hyperparameters for the four outputs after final tuning for the various models. The number of trials adopted for the Bayesian optimization hyperparameter tuning was 100 for all the algorithms.

Table 2. Support vector machine hyperparameter search space

Model Output	Hyperparameter Search Space		
	kernel	C	gamma
Methane Conversion	rbf	[1800, 1900]	[1.4, 1.6]
Hydrogen Yield	rbf	[1800, 1900]	[1.4, 1.6]
Hydrogen Purity	rbf	[33000, 35000]	[6.0, 6.1]
Carbon dioxide Capture	rbf	[33000, 35000]	[6.0, 6.1]

For the SVM models the best hyperparameters for Methane Conversion and Hydrogen Yield were kernel: rbf,; C: 1835; gamma: 1.5276 and Hydrogen Purity and Carbon dioxide Capture: kernel: rbf; C: 33746; gamma: 6.099200124908606 respectively

Table 3. Decision Trees model hyperparameter search space

Model Output	Hyperparameter Search Space		
	max_depth	min_samples_split	min_samples_leaf
Methane Conversion	[40, 70]	[2, 3]	[1, 2]
Hydrogen Yield	[40, 70]	[2, 3]	[1, 2]
Hydrogen Purity	[20, 50]	[2, 4]	[1, 4]
Carbon dioxide Capture	[20, 50]	[2, 4]	[1, 4]

For the Decision Tree models, the best hyperparameters for Methane Conversion and Hydrogen Yield were: max_depth: 40; min_samples_split: 2; min_samples_leaf: 1 and for Hydrogen Purity and Carbon dioxide Capture were max_depth: 37; min_samples_split: 2; min_samples_leaf: 1 respectively

Table 4. Catboost hyperparameter search space

Model Output	Hyperparameter Search Space			
	iterations	depth	l2_leaf_reg	learning_rate
Methane Conversion	[120, 130]	[2, 4]	[1, 2]	[0.02, 0.04]
Hydrogen Yield	[120, 130]	[2, 4]	[1, 2]	[0.02, 0.04]
Hydrogen Purity	[115, 125]	[12, 15]	[1, 2]	[0.02, 0.05]
Carbon dioxide Capture	[1, 100]	[12, 15]	[1, 2]	[0.02, 0.05]

For the Catboost model, the best hyperparameters for Methane Conversion and Hydrogen Yield were iterations: 121; depth: 14; l2_leaf_reg: 1; learning_rate: 0.0348 and for Hydrogen Purity and Carbon dioxide Capture, iterations: 40; depth: 15; l2_leaf_reg: 2; learning_rate: 04232 were observed

Table 5. LightGBM hyperparameter search space

Model Output	Hyperparameter Search Space			
	n_estimators	num_leaves	max_depth	min_data_in_leaf
Methane Conversion	[45, 52]	[2, 4]	[4, 12]	[1, 2]
Hydrogen Yield	[45, 52]	[2, 4]	[4, 12]	[1, 2]
Hydrogen Purity	[45, 65]	[8, 12]	[2, 6]	[1, 3]
Carbon dioxide Capture	[45, 65]	[8, 12]	[2, 6]	[1, 3]

For the LightGBM models the best hyperparameters for Methane conversion and Hydrogen Yield were n_estimators: 52; num_leaves: 4 , max_depth: 4; min_data_in_leaf: 1 while n_estimators: 58; num_leaves: 10; max_depth: 4; min_data_in_leaf: 1 were for Hydrogen Purity and Carbon dioxide Capture respectively

Table 6. Random Forest hyperparameter search space

Model Output	Hyperparameter Search Space			
	n_estimators	max_depth	min_samples_split	min_samples_leaf
Methane Conversion	[15, 26]	[10, 20]	[2, 4]	[1, 3]
Hydrogen Yield	[15, 26]	[10, 20]	[2, 4]	[1, 3]
Hydrogen Purity	[30, 45]	[14, 18]	[2, 3]	[1, 2]
Carbon dioxide Capture	[30, 45]	[14, 18]	[2, 3]	[1, 2]

For the Random Forest models, the best hyperparameters for Methane Conversion and Hydrogen Yield were: n_estimators: 23; max_depth: 17; min_samples_split: 3;min_samples_leaf: 2 while Hydrogen Purity and Carbon dioxide Capture were: n_estimators: 39; max_depth: 15; min_samples_split: 2; min_samples_leaf: 1 respectively.

To evaluate the performance of the models holistically, four metrics were used: coefficient of determination (R^2), Mean Squared Error (MSE), Root Mean Squared Error (RMSE), and Mean Absolute Percentage Error (MAPE). Figures. 10a–f, 12a–f, 14a–f, and 16a–f show the cross plot for the methane conversion, hydrogen yield, hydrogen purity, and carbon dioxide capture efficiency on the train data, while Figures. 11a–f, 13a–f, 15a–f, and 17a–f on the test data.

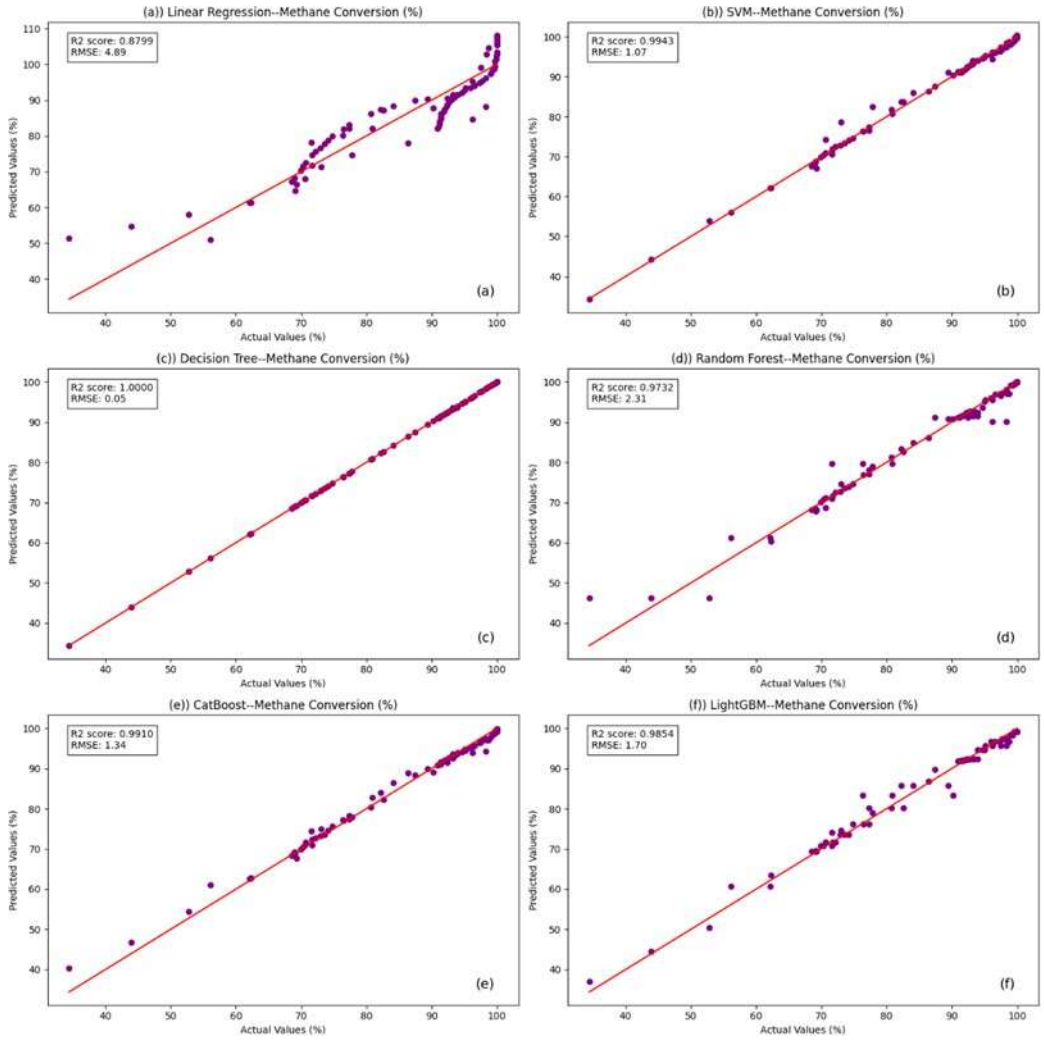


Figure 10a-f. Plot showing the predicted vs actual values on the train data for methane conversion for various models

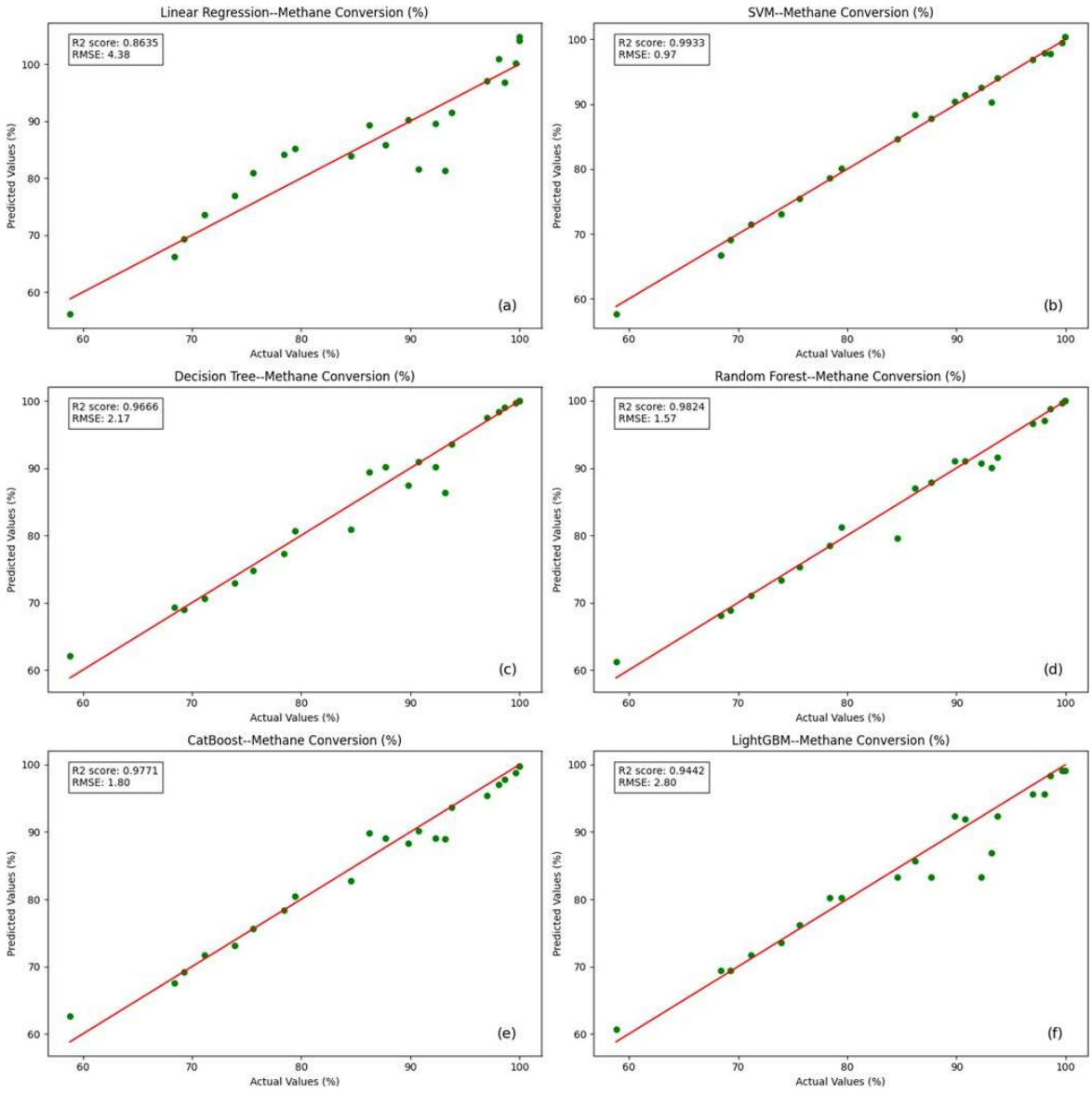


Figure 11a-f. Plot showing the predicted vs actual values on the test data for methane conversion for various models

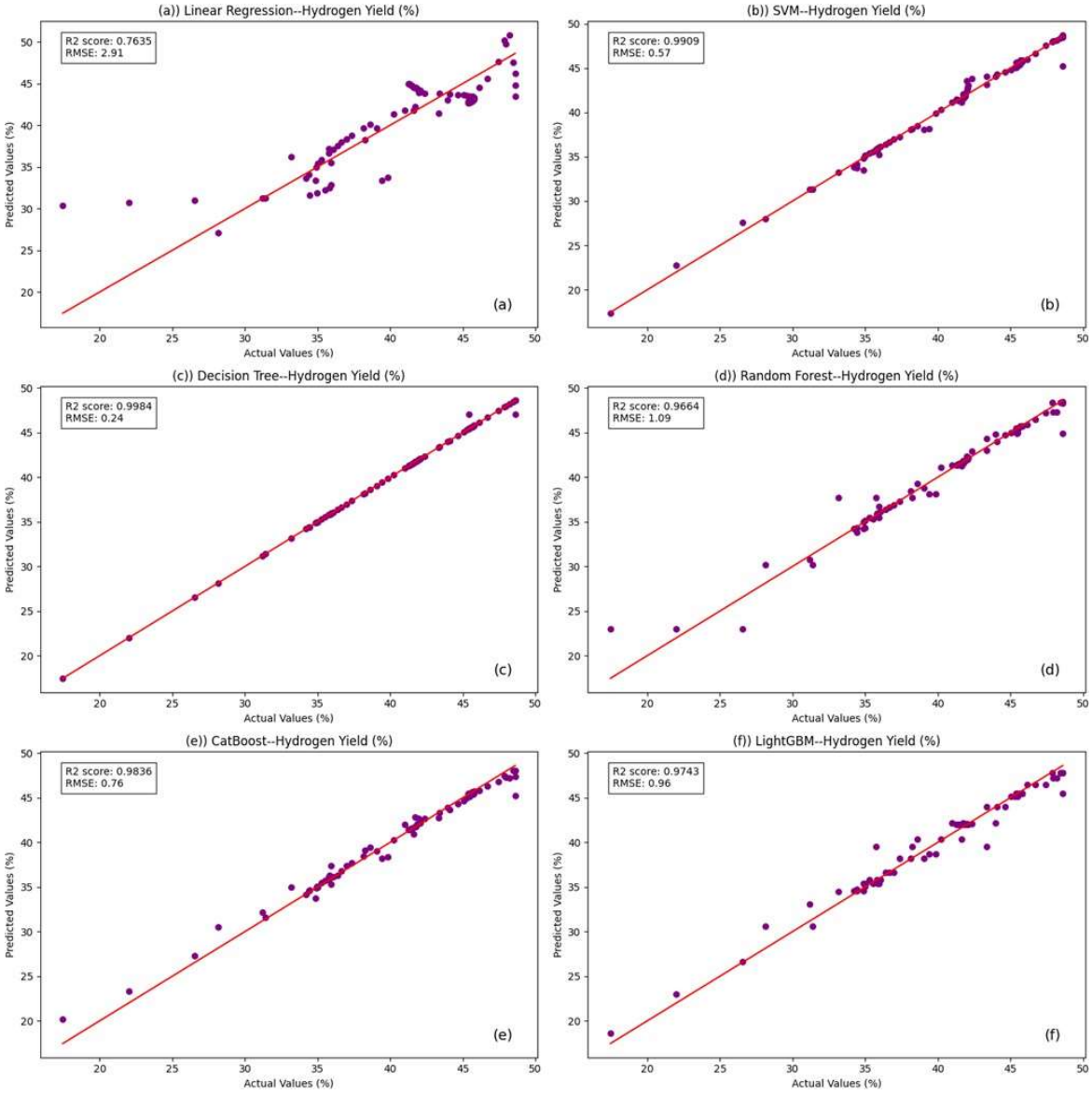


Figure 12a-f. Plot showing the predicted vs actual values on the train data for hydrogen yield for various models

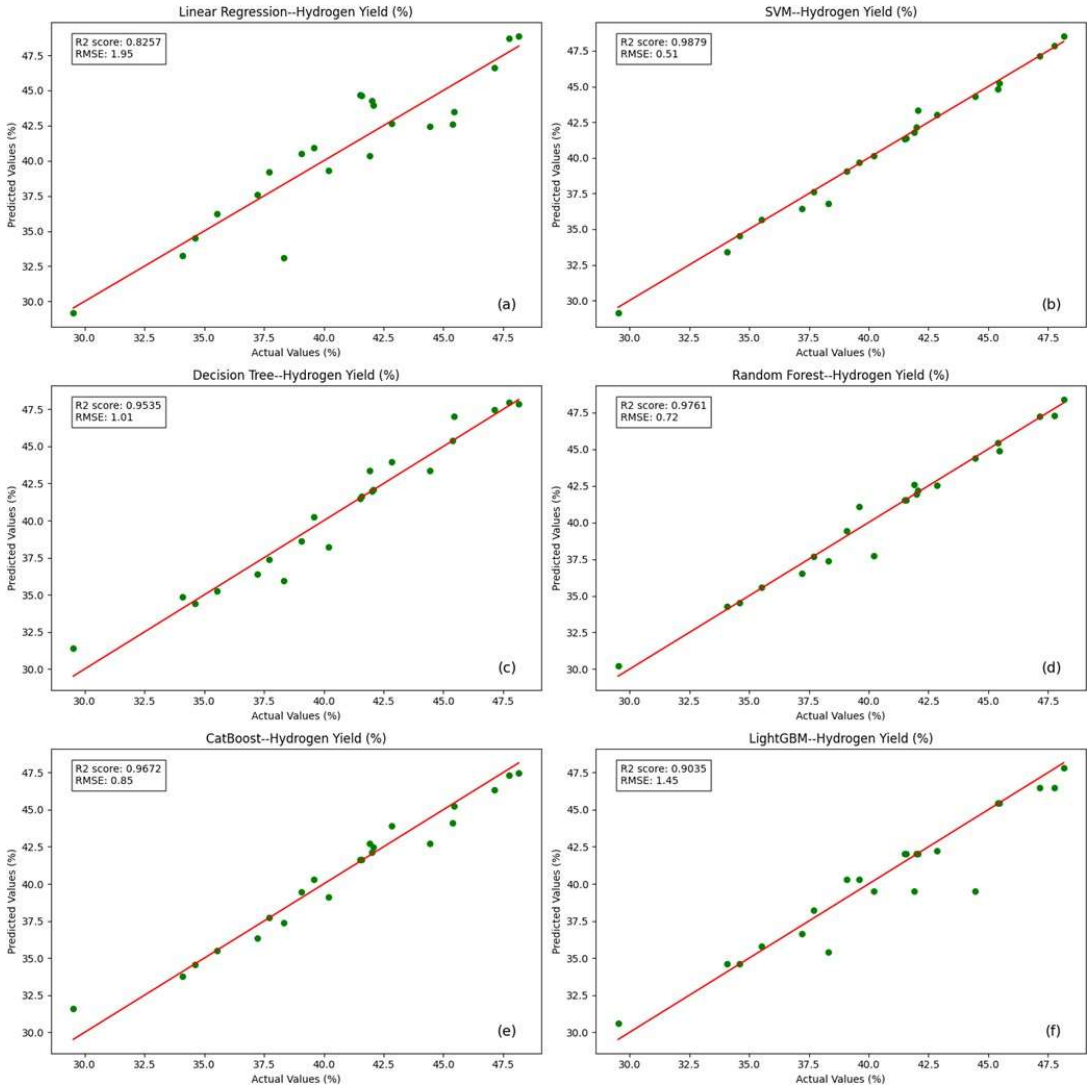


Figure 13a-f. Plot showing the predicted vs actual values on the test data for hydrogen yield for various models

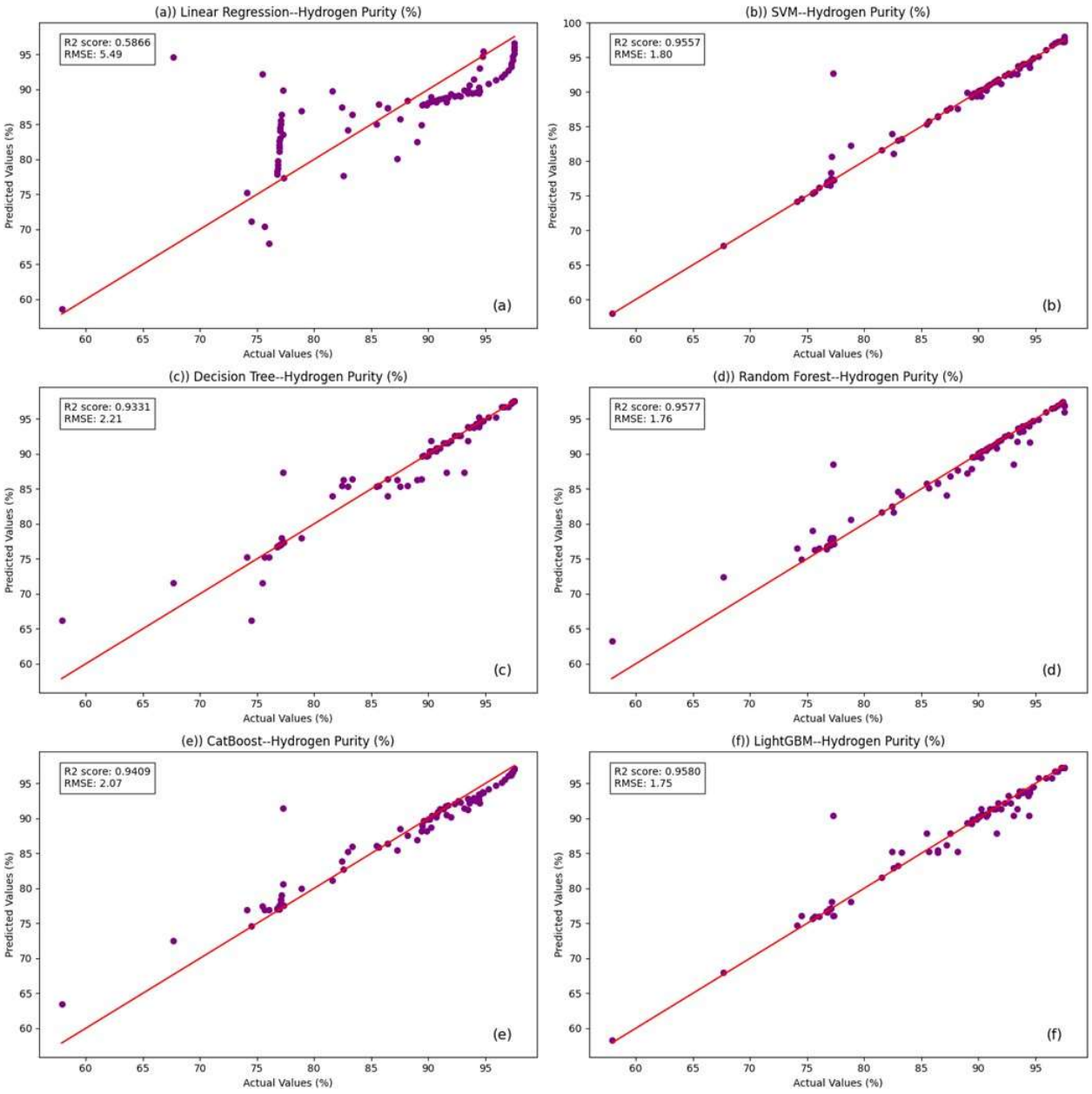


Figure 14a-f. Plot showing the predicted vs actual values on the train data for hydrogen purity for various models

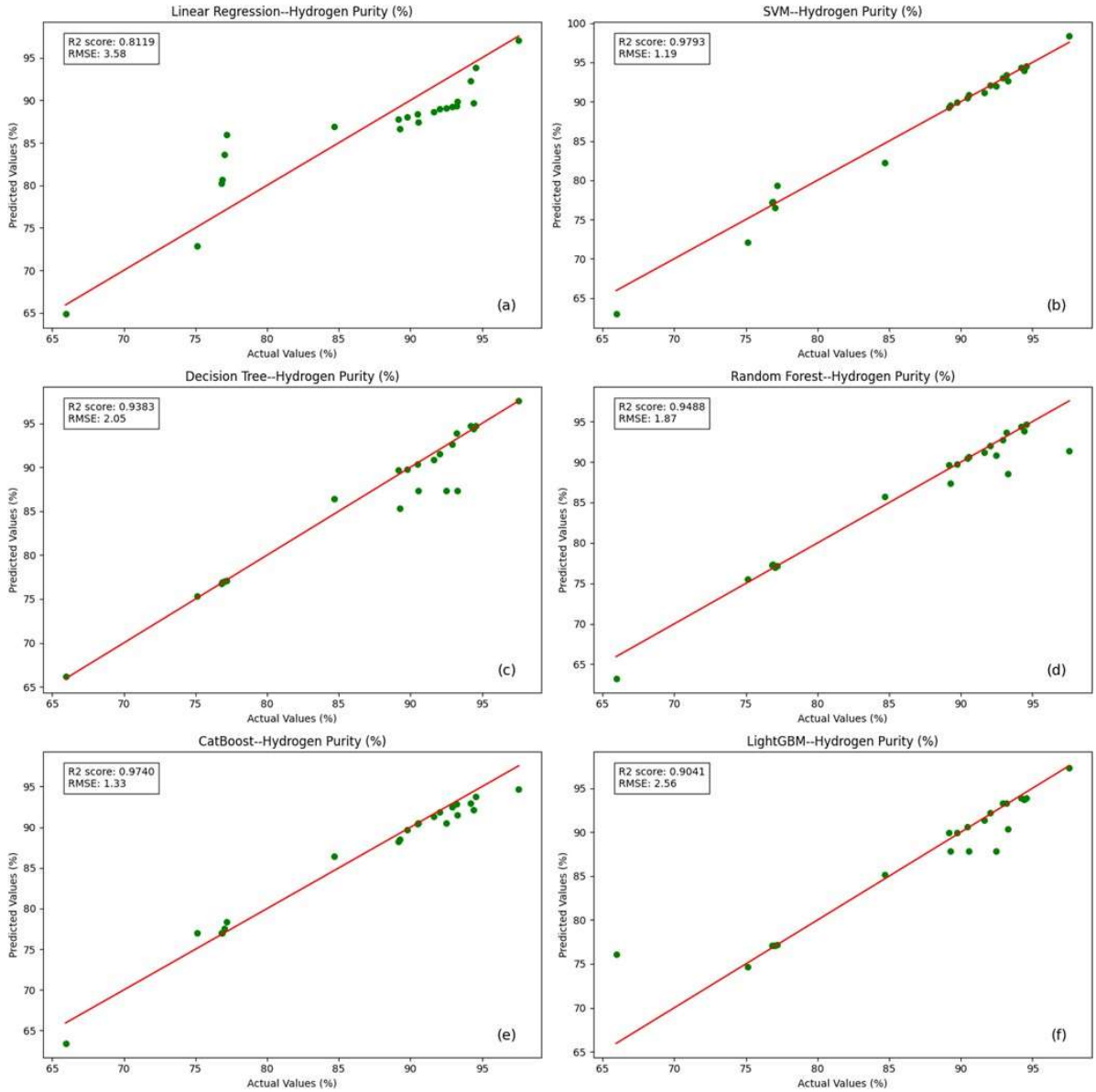


Figure 15a-f. Plot showing the predicted vs actual values on the test data for hydrogen purity for various models

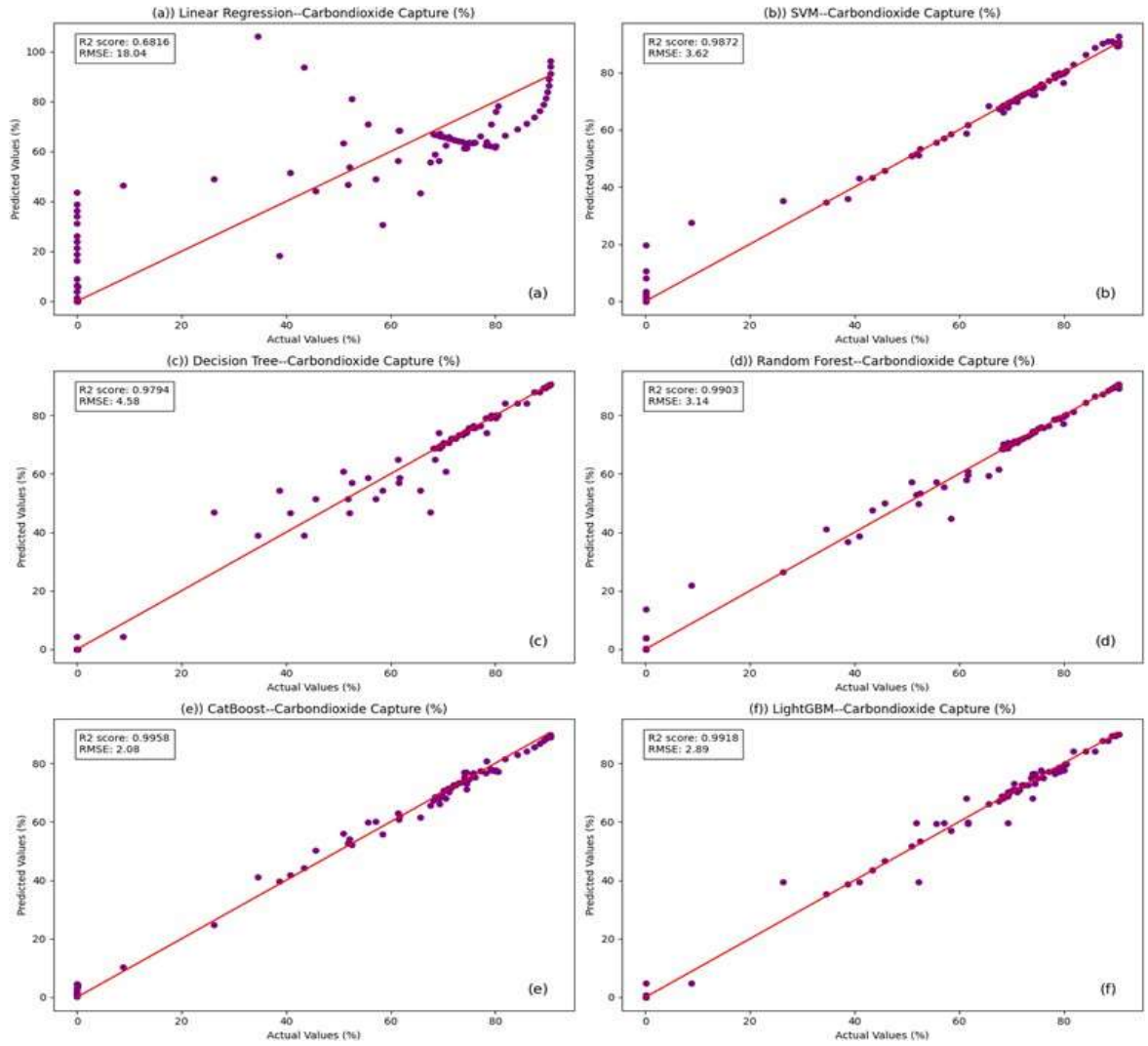


Figure 16a-f. Plot showing the predicted vs actual values on the train data for carbon dioxide capture for various models

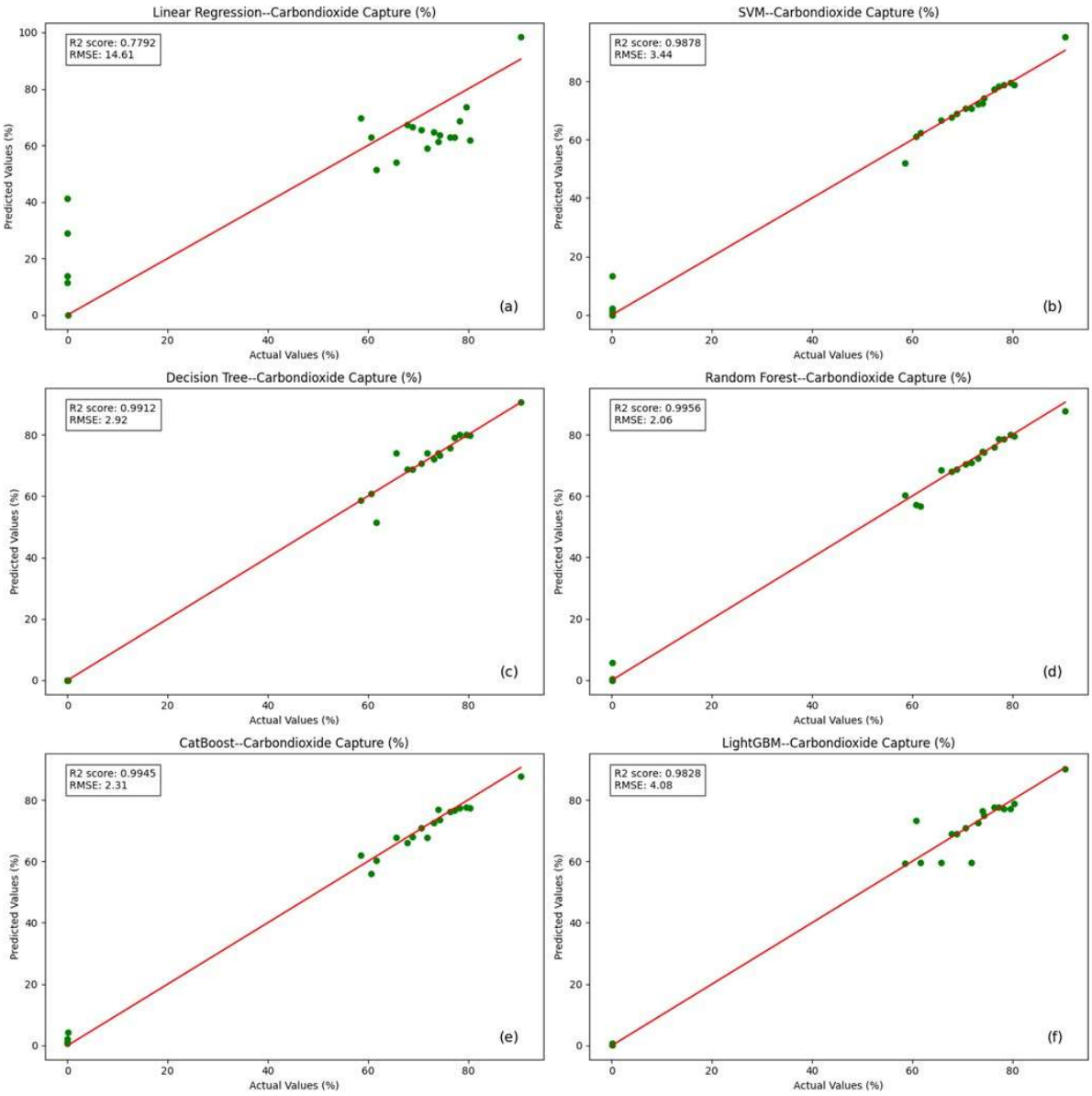


Figure 17a-f. Plot showing the predicted vs actual values on the test data for carbon dioxide capture for various models

Tables 7-10 detail the model performance assessment results on the test data for methane conversion, hydrogen yield, hydrogen purity, and carbon dioxide capture. Table 7 shows that most models, except the linear regression, predicted the methane conversion with relatively high accuracy. The linear regression model achieved an R^2 of 0.864, while LightGBM, decision tree, and Catboost achieved R^2 values of 0.944, 0.967, and 0.982, respectively. The SVM model performed the best, returning an R^2 of 0.993 and an RMSE of 0.973%.

The Firefly-optimised SVM model yielded the highest accuracy in predicting methane conversion in another hydrogen production study conducted by Ehinmowo et al. [19], with an R^2 value of 0.955. The Bayesian-optimised SVM model in this study returned an improved value of 0.993. This demonstrates the effectiveness of SVM in predicting methane conversion. Furthermore, the performance improvement could be attributed to the different optimisation algorithm and the larger dataset employed for this study.

Table 7. Performance of models on the test data for methane conversion.

Model	R-Squared	MSE	RMSE (%)	MAE	MAPE (%)
Linear Regression	0.864	19.221	4.384	3.334	3.92
SVM	0.993	0.947	0.973	0.655	0.798
Decision Tree	0.967	4.703	2.169	1.426	1.735
Random Forest	0.982	2.478	1.574	0.996	1.204
CatBoost	0.977	3.226	1.796	1.285	1.549
LightGBM	0.944	7.853	2.802	1.830	2.094
Ehinmowo et al. (2025)	0.955	50.000	7.070	5.900	9.700

A similar trend is observed in Table 8 where linear regression performed the least in predicting hydrogen yield. LightGBM achieved an R^2 of 0.903, while decision trees reached 0.953. CatBoost and random forest performed even better, with R^2 values of 0.967 and 0.976, respectively.

In the research conducted by Ehinmowo et al. [19], CatBoost achieved the best performance, with an impressive R^2 value of 0.963 in predicting hydrogen yield. Similarly, this study found that CatBoost achieved an R^2 value of 0.967, reinforcing its strength as a reliable model for predicting hydrogen yield. However, it is important to note that the support vector machine (SVM) was found to explain the hydrogen yield variance more effectively in this research, with an R^2 value of 0.988.

Table 8. Performance of models on the test data for hydrogen yield

Model	R-Squared	MSE	RMSE (%)	MAE	MAPE (%)
Linear Regression	0.826	3.801	1.950	1.539	3.747
SVM	0.988	0.264	0.514	0.33	0.841
Decision Tree	0.953	1.015	1.007	0.717	1.849
Random Forest	0.976	0.522	0.722	0.435	1.100
CatBoost	0.967	0.716	0.846	0.648	1.632
LightGBM	0.903	2.105	1.451	0.903	2.221
Ehinmowo et al. (2025)	0.963	40.000	6.400	3.700	8.400

Random forest produced the second-best performance in predicting methane conversion and hydrogen yield. CatBoost outperformed Random Forest in predicting hydrogen purity, achieving an R^2 of 0.974 compared to 0.949 from Random Forest, as shown in Table 9. Although LightGBM returned approximately the same R^2 value for hydrogen yield, it performed worse with higher MSE, MAE, and MAPE values. Linear regression performed the least effectively, while SVM excelled, achieving R^2 values of 0.812 and 0.979, respectively.

Table 9. Performance of models on the test data for hydrogen purity.

Model	R-Squared	MSE	RMSE (%)	MAE	MAPE (%)
Linear Regression	0.812	12.825	3.581	3.07	3.604
SVM	0.979	1.41	1.187	0.735	0.931
Decision Tree	0.938	4.205	2.051	1.101	1.216
Random Forest	0.949	3.493	1.869	1.014	1.156
CatBoost	0.974	1.775	1.332	1.012	1.185
LightGBM	0.904	6.540	2.557	1.239	1.556

A different trend from other process performance indicators was observed in predicting carbon dioxide capture, as shown in Table 10. Although decision tree, catboost, and random forest returned an R^2 above 0.99, the random forest model performed the best, returning 0.996 for R^2, 2.059% for RMSE, 1.281 for MAE, and 1.911% for MAPE. Random Forest returning the best result could be attributed to the kinetically and thermodynamically complex nature of carbon dioxide capture which may require advanced models to better capture the relationships. LightGBM achieved an increased R^2 of 0.983, while linear regression performed the least, returning its lowest R-squared and the highest values for MSE, MAE, and MAPE. The improved performance of LightGBM could also be attributed to the complex nature of carbon dioxide capture suggesting that improved models are required to better predict complicated outputs. Overall, random forest and SVM performed the best since they generally returned the best results for the four outputs across all the performance metrics.

Table 10. Performance of models on the test data for carbon dioxide capture.

Model	R-Squared	MSE	RMSE (%)	MAE	MAPE (%)
Linear Regression	0.779	213.459	14.61	11.514	12.785
SVM	0.988	11.84	3.441	1.761	1.811
Decision Tree	0.991	8.545	2.923	1.33	2.566
Random Forest	0.996	4.241	2.059	1.281	1.911
CatBoost	0.994	5.324	2.307	1.885	2.723
LightGBM	0.983	16.627	4.078	2.146	3.954

3.4. Thermodynamic consistency evaluation

Since the equilibrium compositions were calculated by minimising Gibbs free energy for both simulation studies, the thermodynamic consistency of the predictions were evaluated by comparing the

predicted values with the simulated values in the dataset.

The results were similar with the thermodynamically expected values and was also within the physical boundaries of the outputs. For example, the actual methane conversion at a reformer temperature of 859.37℃; pressure of 1.01 bar; S/C of 3; and CaO/C of 1 was 99.99%. The predicted values for decision trees, random forest, catboost, and lightgbm were 99.97%, 99.98%, 99.67%, and 99.43% respectively.

3.5. Feature importance evaluation

A feature importance plot was created to understand the degree of contribution of each feature in predicting the four process performance indicators. Figure 18a–d shows a feature importance plot for methane conversion. All the models except lightGBM produced a similar order, with the reformer pressure contributing the most.

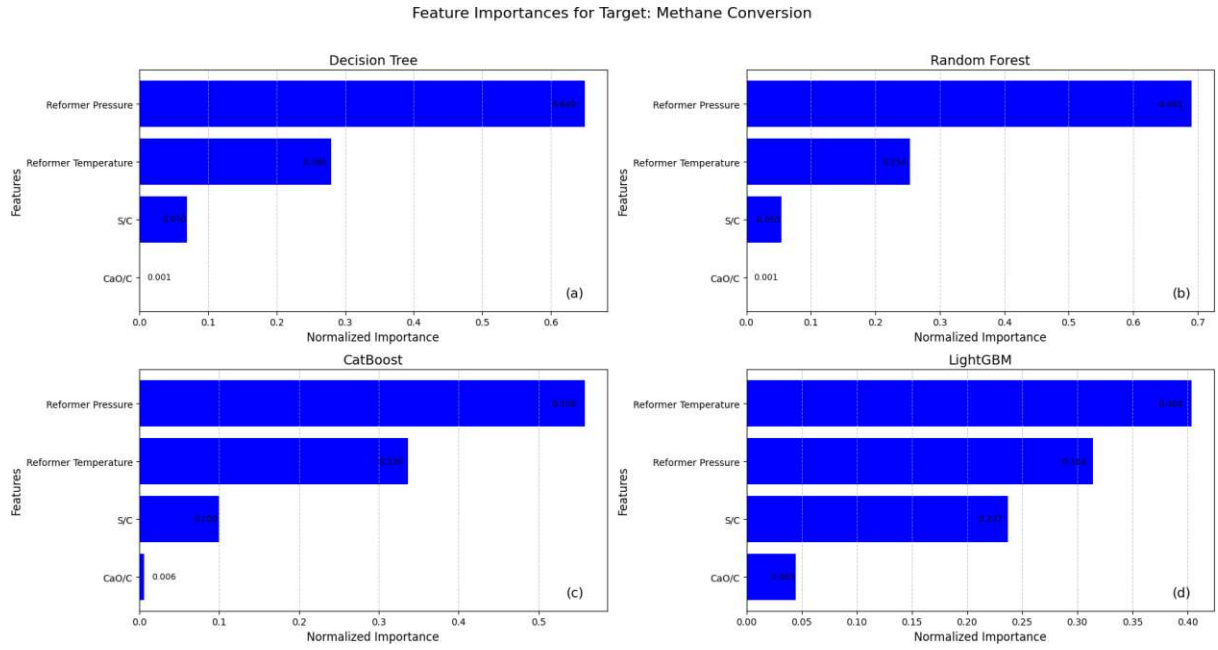


Figure 18a-d. Feature importance plot for methane conversion for various models

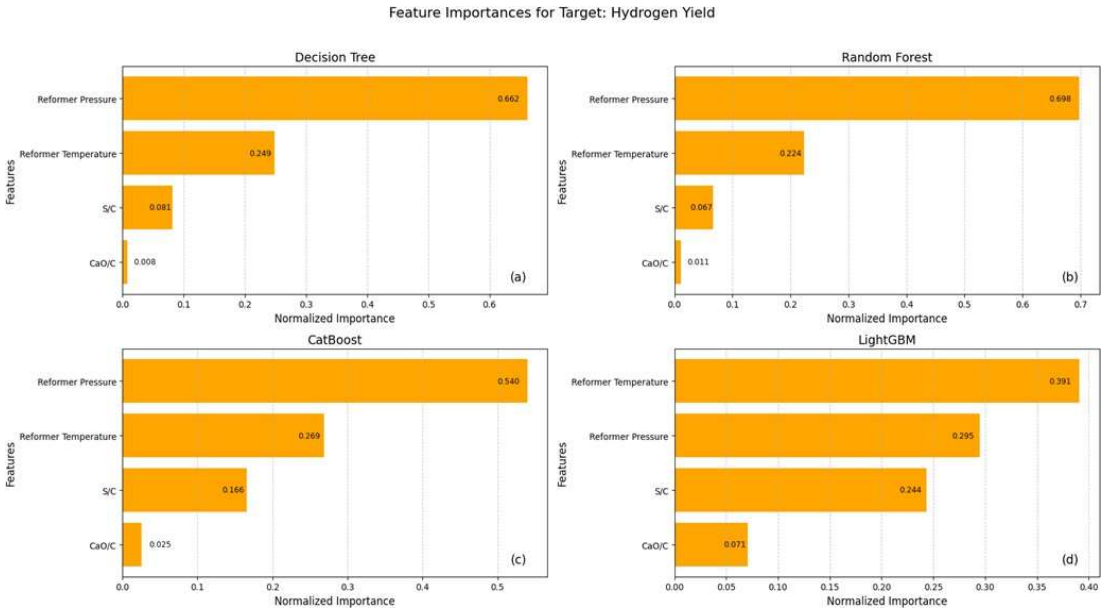


Figure 19a-d. Feature importance plot for hydrogen yield for various models

The feature importance plots for various models regarding hydrogen yield are illustrated in Figure 19a–d. The order is similar to the feature importance for methane conversion, with lightGBM returning a different result, where reforming temperature is the most important feature.

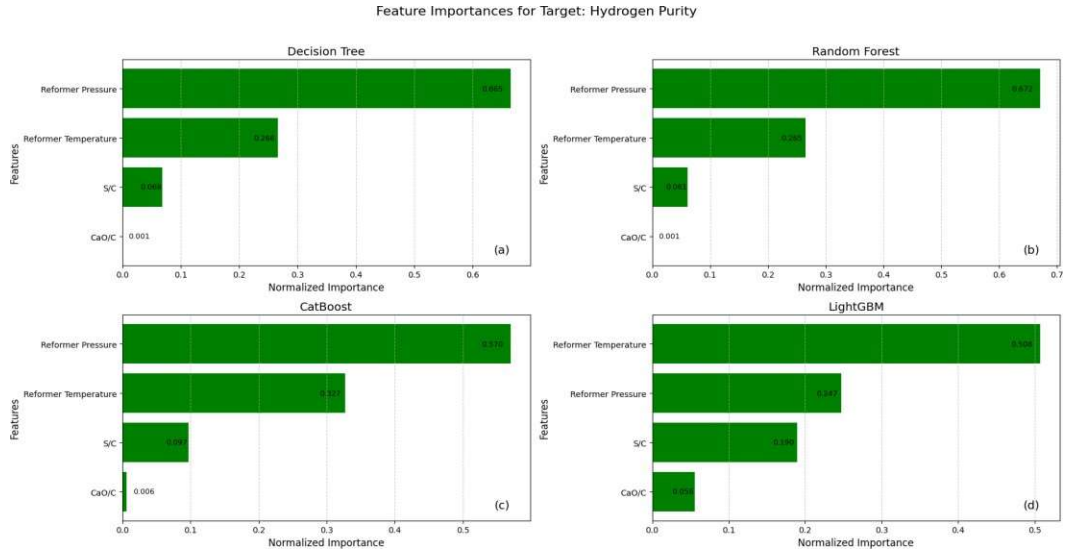


Figure 20a-d. Feature importance plot for hydrogen purity for the various models

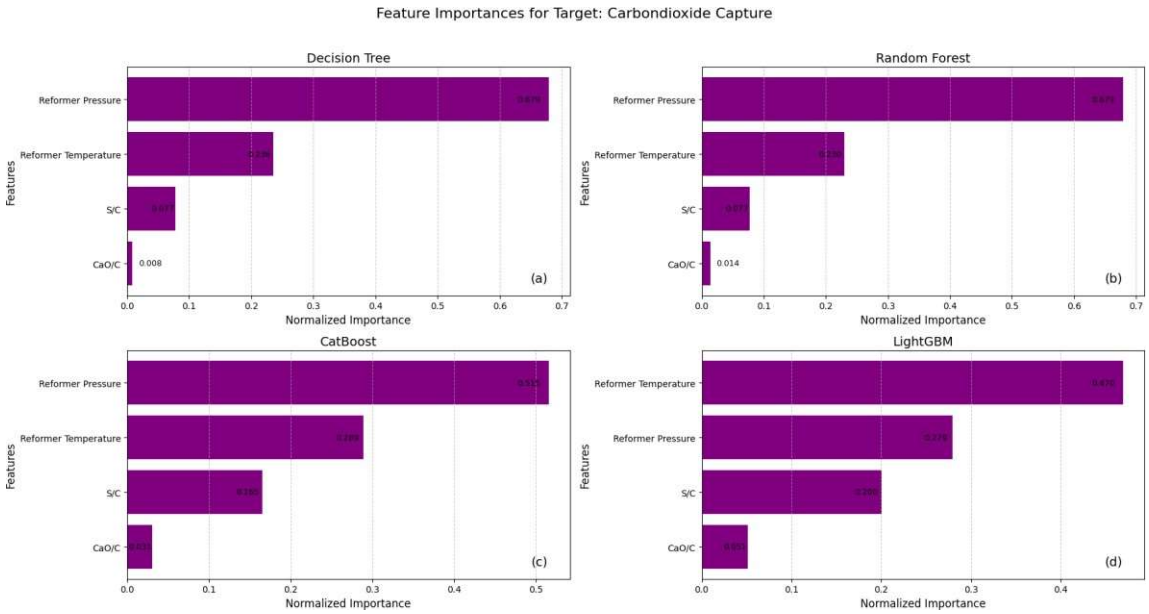


Figure 21a-d. Feature importance plot for carbon dioxide capture for the various models

Figures 20a–d and 21a–d show the feature importance plots for hydrogen purity and carbon dioxide capture. The same pattern continued, with similar ordering but different magnitudes for the decision tree, random forest, and CatBoost models. In contrast, lightGBM produced a different yet consistent order, highlighting that the reformer temperature had the most significant impact.

4. Conclusion

This study integrates an optimisation algorithm with various machine learning models using a dual multi-output approach to predict four crucial process outputs: methane conversion, hydrogen yield, hydrogen purity, and carbon dioxide capture. The models demonstrated high predictive accuracy, with most achieving a coefficient of determination above 90% and a low root mean square error. Support vector machines showed the highest effectiveness in predicting methane conversion, hydrogen yield, and hydrogen purity, achieving R^2 values of 0.993, 0.988, and 0.979, respectively. The SVM model reported RMSE values of 0.973%, 0.514%, and 1.187%, respectively. The high R^2 values and low root mean square error values denote strong performance of the models. Random forest was a close second in predicting methane conversion and hydrogen yield, returning R^2 values of 0.982 and 0.976. The CatBoost model achieved the second-best predictive performance in hydrogen purity and carbon dioxide capture, with R^2 values of 0.974 and 0.994. Random forest performed the best in predicting carbon dioxide capture with an R^2 of 0.996 and an RMSE of 2.059%. The strong performance of these models advances the progress towards real-time monitoring of sorption-enhanced steam methane reforming outputs using machine learning techniques. Future study could evaluate multi-objective optimisation among these outputs using machine learning methods.

Conflict of Interest

We declare no conflict regarding the publication of the study.

References

[1] Energy Institute. (2024). *Statistical review of world energy 2024* (73rd ed.). https://www.energyinst.org/data/assets/pdf_file/0006/1542714/684_EI_Stat_Review_V16_DIGITAL.pdf

[2] Calvin, K., Dasgupta, D., Krinner, G., Mukherji, A., Thorne, P. W., Trisos, C., Romero, J., Aldunce, P., Barrett, K., Blanco, G., Cheung, W. W. L., Connors, S., Denton, F., Diongue-Niang, A., Dodman, D., Garschagen, M., Geden, O., Hayward, B., Jones, C., Péan, C. (2023). *IPCC, 2023: Climate Change 2023: Synthesis Report. Contribution of Working Groups I, II and III to the Sixth Assessment Report of the Intergovernmental Panel on Climate Change [Core Writing Team, H. Lee and J. Romero (eds.)]. IPCC, Geneva, Switzerland.* Intergovernmental Panel on Climate Change. https://doi.org/10.59327/ipcc/ar6-9789291691647

[3] Bolan, S., Padhye, L. P., Jasemizad, T., Govarthanan, M., Karmegam, N., Wijesekara, H., Amarasiri, D., Hou, D., Zhou, P., Biswal, B. K., Balasubramanian, R., Wang, H., Siddique, K. H. M., Rinklebe, J., Kirkham, M. B., & Bolan, N. (2024). Impacts of climate change on the fate of contaminants through extreme weather events. *Science of The Total Environment*, *909*, 168388. https://doi.org/10.1016/j.scitotenv.2023.168388

[4] United Nations. (n.d.). *Causes and Effects of Climate Change*. Retrieved July 13, 2025, from https://www.un.org/en/climatechange/science/causes-effects-climate-change

[5] Ember. (2024). *Global electricity review 2024*. https://ember-climate.org/insights/research/global-electricity-review-2024/

[6] Sadeq, A. M., Homod, R. Z., Hussein, A. K., Togun, H., Mahmoodi, A., Isleem, H. F., Patil, A. R., & Moghaddam, A. H. (2024). Hydrogen energy systems: Technologies, trends, and future prospects. *Science of The Total Environment*, *939*, 173622. https://doi.org/10.1016/j.scitotenv.2024.173622

[7] Szablowski, L., Wojcik, M., & Dybinski, O. (2025). Review of steam methane reforming as a method of hydrogen production. *Energy*, *316*, 134540. https://doi.org/10.1016/j.energy.2025.134540

[8] Soltani, R., Rosen, M. A., & Dincer, I. (2014). Assessment of CO_2 capture options from various points in steam methane reforming for hydrogen production. *International Journal of Hydrogen Energy*, *39*(35), 20266–20275. https://doi.org/10.1016/j.ijhydene.2014.09.161

[9] Hildenbrand, N., Readman, J., Dahl, I. M., & Blom, R. (2006). Sorbent enhanced steam reforming (SESR) of methane using dolomite as internal carbon dioxide absorbent: Limitations due to $Ca(OH)_2$ formation. *Applied Catalysis A: General*, *303*(1), 131–137. https://doi.org/10.1016/j.apcata.2006.02.015

[10] Mostafa, A., Rapone, I., Bosetti, A., Romano, M. C., Beretta, A., & Groppi, G. (2023). Modelling of methane sorption enhanced reforming for blue hydrogen production in an adiabatic fixed bed reactor: Unravelling the role of the reactor's thermal behaviour. *International Journal of Hydrogen Energy*, *48*(68), 26475–26491. https://doi.org/10.1016/j.ijhydene.2023.03.357

[11] Choi, D. H., Chun, S. M., Ma, S. H., & Hong, Y. C. (2016). Production of hydrogen-rich syngas from methane reforming by steam microwave plasma. *Journal of Industrial and Engineering Chemistry*, *34*, 286–291. https://doi.org/10.1016/j.jiec.2015.11.019

[12] Abbas, S. Z., Dupont, V., & Mahmud, T. (2019). Modelling of H_2 production via sorption-enhanced steam methane reforming at reduced pressures for small-scale applications. *International Journal of Hydrogen Energy*, *44*(3), 1505–1513. https://doi.org/10.1016/j.ijhydene.2018.11.169

[13] Teixeira, P., Bacariza, C., Correia, P., Pinheiro, C. I. C., & Cabrita, I. (2022). Hydrogen production with in situ CO_2 capture at high and medium temperatures using solid sorbents. *Energies*, *15*(11), 4039. https://doi.org/10.3390/en15114039

[14] Hosseinzadeh, A., Zhou, J. L., Altaee, A., & Li, D. (2022). Machine learning modelling and analysis of biohydrogen production from wastewater by dark fermentation process. *Bioresource Technology*, *343*, 126111. https://doi.org/10.1016/j.biortech.2021.126111

[15] Ozbas, E. E., Aksu, D., Ongen, A., Aydin, M. A., & Ozcan, H. K. (2019). Hydrogen production via biomass gasification, and modelling by supervised machine learning algorithms. *International Journal of Hydrogen Energy*, *44*(32), 17260–17268. https://doi.org/10.1016/j.ijhydene.2019.02.108

[16] Alsaffar, M. A., Ghany, M. A. R. A., Ali, J. M., Ayodele, B. V., & Mustapa, S. I. (2021). Artificial neural network modelling of thermo-catalytic methane decomposition for hydrogen production. *Topics in Catalysis*, *64*(5), 456–464. https://doi.org/10.1007/s11244-020-01409-6

[17] Nkulikiyinka, P., Yan, Y., Güleç, F., Manovic, V., & Clough, P. T. (2020). Prediction of sorption enhanced steam methane reforming products from machine learning based soft-sensor models. *Energy and AI*, *2*, 100037. https://doi.org/10.1016/j.egyai.2020.100037

[18] Wang, L., Li, H., Du, C., & Hong, W. (2024). Sorption-enhanced steam methane reforming parameter analysis and performance prediction of ensemble learning methods using an improved drag model. *Advanced Powder Technology*, *35*(8), 104576. https://doi.org/10.1016/j.apt.2024.104576

[19] Ehinmowo, A. B., Nwaneri, B. I., & Olaide, J. O. (2025). Predictive modelling of hydrogen production and methane conversion from biomass-derived methane using machine learning and optimisation techniques. *Next Energy*, *7*, 100229. https://doi.org/10.1016/j.nxener.2024.100229

[20] Bishnu, S.K., Alnouri, S.Y., & Al Mohannadi, D. M. (2025). Stochastic algorithm-based optimisation using artificial intelligence/machine learning models for sorption-enhanced steam methane reformer reactor. *Computers & Chemical Engineering*, *196*, 109060. https://doi.org/10.1016/j.compchemeng.2025.109060

[21] Antzara, A., Heracleous, E., Bukur, D. B., & Lemonidou, A. A. (2014). Thermodynamic analysis of hydrogen production via chemical looping steam methane reforming coupled with in Situ CO_2 c apture. *Energy Procedia*, *63*, 6576–6589. https://doi.org/10.1016/j.egypro.2014.11.694

[22] Faheem, H. H., Tanveer, H. U., Abbas, Syed. Z., & Maqbool, F. (2021). Comparative study of conventional steam-methane-reforming (SMR) and auto-thermal-reforming (ATR) with their hybrid sorption enhanced (SE-SMR & SE-ATR) and environmentally benign process models for the hydrogen production. *Fuel*, *297*, 120769. https://doi.org/10.1016/j.fuel.2021.120769

[23] Costa, L. A. L. F. da, Kunst, R., & de Freitas, E. P. (2022). Intelligent resource sharing to enable quality of service for network clients: The trade-off between accuracy and complexity. *Computing*, *104*(5), 1219– 1231. https://doi.org/10.1007/s00607-021-01042-5

[24] Rivera-Lopez, R., Canul-Reich, J., Mezura-Montes, E., & Cruz-Chávez, M. A. (2022). Induction of decision trees as classification models through metaheuristics. *Swarm and Evolutionary Computation*, *69*, 101006. https://doi.org/10.1016/j.swevo.2021.101006

[25] Yazdani, H., Doostizadeh, M., & Aminifar, F. (2023). Forecast-aided power and flexibility trading of prosumers in peer-to-peer markets. *IET Renewable Power Generation*, *17*(4), 920–934. https://doi.org/10.1049/rpg2.12645

[26] Manjrekar, O. N., & Dudukovic, M. P. (2019). Identification of flow regime in a bubble column reactor with a combination of optical probe data and machine learning technique. *Chemical Engineering Science: X*, *2*, 100023. https://doi.org/10.1016/j.cesx.2019.100023

[27] Liu, M., Liu, X., Li, J., Ding, C., & Jiang, J. (2014). Evaluating total inorganic nitrogen in coastal waters through fusion of multi-temporal RADARSAT-2 and optical imagery using random forest algorithm. *International Journal of Applied Earth Observation and Geoinformation*, *33*, 192–202. https://doi.org/10.1016/j.jag.2014.05.009

[28] Pandey, M., Karbasi, M., Jamei, M., Malik, A., & Pu, J. H. (2023). A comprehensive experimental and computational investigation on estimation of scour depth at bridge abutment: Emerging ensemble intelligent systems. *Water Resources Management*, *37*(9), 3745–3767. https://doi.org/10.1007/s11269-023- 03525-w

[29] Light Gradient Boosting Machine 4.6.0.99 documentation. Retrieved July 11, 2025, from https://lightgbm.readthedocs.io/en/latest/Features.html

[30] Li, Y., Zhang, Y., & Cai, Y. (2021). A new hyperparameter optimisation method for power load forecast

based on recurrent neural networks. *Algorithms*, *14*(6), 163. https://doi.org/10.3390/a14060163

[31] Johnsen, K., Ryu, H. J., Grace, J. R., & Lim, C. J. (2006). Sorption-enhanced steam reforming of methane in a fluidized bed reactor with dolomite as CO_2 -acceptor. *Chemical Engineering Science*, *61*(4), 1195–1202. https://doi.org/10.1016/j.ces.2005.08.022